Computing Arnol′d tongue scenarios

Frank Schilder [a,*], Bruce B. Peckham [b]

[a] *Bristol Centre for Applied Nonlinear Mathematics, Department of Engineering Mathematics, University of Bristol, Bristol BS8 1TR, UK*
[b] *Department of Mathematics and Statistics, 140 Solon Campus Center, University of Minnesota – Duluth,*
1117 University Dr., Duluth, MN 55812-3000, USA

Abstract

A famous phenomenon in circle-maps and synchronisation problems leads to a two-parameter bifurcation diagram commonly referred to as the Arnol′d tongue scenario. One considers a perturbation of a rigid rotation of a circle, or a system of coupled oscillators. In both cases we have two natural parameters, the coupling strength and a detuning parameter that controls the rotation number/frequency ratio. The typical parameter plane of such systems has Arnol′d tongues with their tips on the decoupling line, opening up into the region where coupling is enabled, and in between these Arnol′d tongues, quasi-periodic arcs. In this paper, we present unified algorithms for computing both Arnol′d tongues and quasi-periodic arcs for both maps and ODEs. The algorithms generalise and improve on the standard methods for computing these objects. We illustrate our methods by numerically investigating the Arnol′d tongue scenario for representative examples, including the well-known Arnol′d circle map family, a periodically forced oscillator caricature, and a system of coupled Van der Pol oscillators.
© 2006 Elsevier Inc. All rights reserved.

1. Introduction

Many interesting problems in science and engineering lead to models involving either periodically forced oscillators or coupled oscillators. Natural parameters to vary in the periodically forced oscillator setting are the forcing amplitude and the forcing period/frequency. In the coupled oscillator setting, coupling strength is a natural parameter, with a typical second parameter, often referred to as a ''detuning'' parameter, controlling the relative frequencies of the two coupled oscillators. The two settings can be unified by viewing periodically forced oscillators as coupled oscillators, with one-way coupling – the forcing amplitude corresponding to the coupling strength.

---

* Corresponding author.
  E-mail addresses: f.schilder@bristol.ac.uk (F. Schilder), bpeckham@d.umn.edu (B.B. Peckham).

The most prominent phenomenon in these systems is the transition between phase locking (also called entrainment or synchronisation) and quasi-periodicity. Phase locking produces a periodic solution which generically persists as parameters are varied. In contrast, quasi-periodicity is a codimension-one phenomenon which is thus generically destroyed by perturbation. The result is a well-known bifurcation diagram in the two-parameter plane called the "Arnol'd tongue" scenario [1–6,14,17,18,21,26,28,29,37]. It has a countable collection of Arnol'd tongues, emanating from "rational" points on the zero forcing/coupling axis, and opening up into regions where the coupling strength is turned on. Each tongue corresponds to phase locked solutions for which the two frequencies of the oscillators satisfy $\omega_1/\omega_2 = p/p$ for some integers p and q. In between the tongues, emanating from all the "irrational" points on the zero forcing/amplitude axis, are curves of parameters corresponding to quasi-periodic flow on a torus with an irrational frequency ratio ω_1/ω_2. This scenario is generic for weakly coupled oscillators [1,5]. A similar – but not identical – Arnold tongue scenario occurs in the neighbourhood of a Neimark–Sacker curve [6,26,37]. We focus in this paper on continuation from zero forcing amplitude, but arrive at a Neimark–Sacker curve by continuation in the second and third of our three examples in Section 4. Look ahead to examples of these two-parameter bifurcation diagrams in Figs. 5, 9, 13.

There is a variety of ways in which we can model coupled oscillators. The simplest is as a flow in $\mathbb{S} \times \mathbb{S}$. Embedding each oscillator in $\mathbb{R}^{n_i}$, $i = 1,2$, leads to the more general setting of a flow in $\mathbb{R}^{n_1} \times \mathbb{R}^{n_2}$. In the decoupled case this flow has an invariant two-torus, which is the product of two limit cycles of the individual oscillators. Assuming these limit cycles are hyperbolic attractors, this two-torus will persist, at least for small coupling strengths. This flow in $\mathbb{R}^{n_1} \times \mathbb{R}^{n_2}$ is often studied by reduction to a Poincaré return map of $\mathbb{R}^{n_1+n_2-1}$ by sampling the state of the system, for example, as it passes in a specified direction through a well-chosen hyperplane. In the periodically forced oscillator case, this return map can be further reduced to a simple stroboscopic map of the flow in $\mathbb{R}^{n_1}$ at the time period of the uncoupled limit cycle in $\mathbb{R}^{n_2}$. This is possible because the flow in $\mathbb{R}^{n_2}$ is decoupled from the flow in $\mathbb{R}^{n_1}$. The reduction can also be thought of as from a periodic non-autonomous flow in $\mathbb{R}^{n_1}$ to an autonomous map in $\mathbb{R}^{n_1}$. The invariant two-torus in the original flow becomes an invariant circle for either the Poincaré map of $\mathbb{R}^{n_1+n_2-1}$ or the stroboscopic map of $\mathbb{R}^{n_1}$. This allows one further reduction, by restricting attention to the invariant circle, from the maps of $\mathbb{R}^n$ to circle maps. This is the motivation for the Arnol'd sine circle map family which we study in Section 4.1.

Because the invariant circle is not guaranteed to persist globally in the parameter space, we study a more general family in Section 4.2. This family is intended to exhibit generic properties of a Poincaré return map generated by a periodically forced planar oscillator. We call this map the periodically forced oscillator caricature map family. It has been studied previously in [27,28,31,32]. Note that both the Arnol'd circle maps and the caricature maps provide a significant computational shortcut by defining the maps directly, rather than requiring integration of differential equations to define each iterate. Our third family, however, a system of two linearly coupled Van der Pol oscillators, is defined directly from the following system of differential equations:

$$\ddot{x} + \varepsilon(x^2 - 1)\dot{x} + x = \alpha(y - x),$$
$$\ddot{y} + \varepsilon(y^2 - 1)\dot{y} + (1 + \beta)y = \alpha(x - y),$$

We look briefly at this system now, to preview some of the main results of the paper. Specifically, we compare the computation of certain Arnol'd tongues via traditional methods with the computational algorithms introduced in this paper.

The coupled Van der Pol system has been studied previously in [17,34,36]. We re-investigate it in more depth in Section 4.3. This system is in the coupled oscillator setting introduced above, with coupling strength α and the detuning parameter β. Hence, the (β, α) parameter plane exhibits the Arnol'd tongue scenario and our goal is to compute a preferably large set of these tongues. Since the boundaries of an Arnol'd tongue are loci of saddle-node or fold bifurcations [2,3,17], we used the continuation package AUTO [16] to compute such fold curves for several Arnol'd tongues. A standard method for computing an Arnol'd tongue is to locate a periodic point in the tongue, follow it to a saddle-node bifurcation, and then switch to continue the saddle-node bifurcation curve in α and β as the boundary of the tongue. Fig. 1 shows the first six tongues corresponding to the periods 1, 2, 3, 4 and 5. We found it not only very hard to obtain suitable start data, but we were also unable to continue the curves all the way down to the zero coupling line $\alpha = 0$. This is not due to a limitation
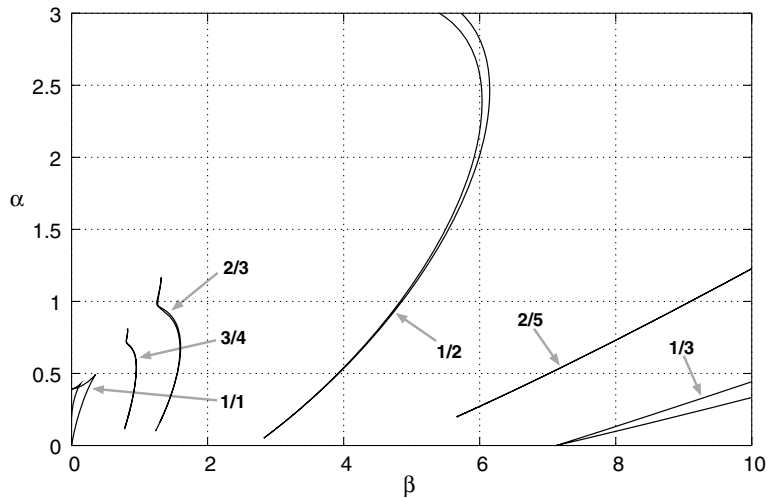
Fig. 1. Some Arnol'd tongues of the system of two coupled Van der Pol oscillators for $\varepsilon = 1$, computed by fold continuation. Numerical problems prevented most continuations from reaching $\alpha = 0$.

of the package AUTO [16]. The continuation of saddle-node curves seems to be ill-posed near the line $\alpha = 0$ because the tongues are so narrow. Although the tongues generically open at a finite angle [18], the angle decreases, and therefore the ill-posedness becomes worse, as the period q of the Arnold tongue increases. We also note that the generic finite angle condition often fails in common examples such as the Arnold sine map discussed in Section 4.1 due to the finite Fourier series expansion of the forcing function $\sin(x)$. The continuation problems illustrated in Fig. 1 should be compared with the results of our algorithms displayed in Fig. 13, where we display a large set of tongues, each one continued from $\alpha = 0$.

In this paper, we present algorithms that allow the numerical investigation of the Arnol'd tongue scenario in a two-parameter plane. More precisely, we consider two-parameter families of maps

$$x \mapsto f(x, \alpha, \beta), \quad f : \mathbb{R}^n \times \mathbb{R} \times \mathbb{R} \to \mathbb{R}^n, \tag{1}$$

and two-parameter families of ordinary differential equations (ODEs)

$$\dot{x} = f(x, \alpha, \beta), \quad f : \mathbb{R}^n \times \mathbb{R} \times \mathbb{R} \to \mathbb{R}^n, \tag{2}$$

where f is in both cases sufficiently smooth in all arguments. That is, the map f in (1) is at least of class $\mathscr{C}^2$ and the right-hand side f in (2) is at least of class $\mathscr{C}^{1+L}$. Both functions are assumed to have a higher degree of smoothness if required by a numerical procedure that we employ. Throughout this paper we assume that the parameter α plays the role of a coupling strength and that β is a detuning parameter controlling the ratio of frequencies in the system. The systems are assumed to have an invariant torus at $\alpha = 0$, most commonly an invariant circle in the map setting, and an invariant two-torus in the ODE setting. These two general settings include all the scenarios discussed above in this introduction. In both settings the (β, α) parameter plane features Arnol'd tongues with tips at the line $\alpha = 0$.

The computations of Arnol'd tongues and quasi-periodic arcs are two-parameter continuations by nature [2,3,17,36]. In all the considerations that follow, we aim at using pseudo arc-length continuation. That is, we derive algebraic systems that have one more variable than equations, where the variables include both parameters α and β. Our arc-length continuation method automatically amends these systems with a so-called arc-length condition, which leads to systems of equations that have as many variables as equations. The arc-length continuation method is well-posed if the objects that are continued form a $\mathscr{C}^1$-family in combined parameter and phase space. Our method for Arnol'd tongues continues families of periodic orbits and differentiability of these families is a standard result under our assumptions made above. That quasi-periodic arcs are smooth as well is less trivial and differentiability results can be found in, for example [7,8].

In Section 2, we generalise ideas introduced previously [27,32] and construct algorithms for Arnol'd tongues for general n-dimensional maps and ODEs. In Section 3, we combine ideas in [10,22,36] with a two-point

boundary value problem setting and continuation techniques to compute quasi-periodic arcs that sit in between the Arnol′d tongues. The performance of our methods is demonstrated with three examples in Section 4: an embedded Arnol′d family in Section 4.1, a generic caricature example in Section 4.2 and the system of coupled Van der Pol oscillators in Section 4.3. We conclude our paper in Section 5 with a discussion and some future directions.

2. Computation of Arnol′d tongues

For simplicity, we first restrict our discussion to the map case and assume a one-dimensional invariant circle at $\alpha = 0$. In this setting, an Arnol′d tongue can be considered as the projection of a so-called resonance surface to the two-parameter plane [27,28,31,32]. A "p/q resonance surface" is defined as the connected component in the phase × parameter space $\mathbb{R}^n \times \mathbb{R} \times \mathbb{R}$ of period-q points with rotation number p/q, that is, as a connected set of zeroes of $f^q(x, \alpha, \beta) - x$. Assuming the invariant circle is normally hyperbolic and that the rotation number is a hyperbolically monotonic function of β at $\alpha = 0$, the implicit function theorem guarantees that the local continuation of the surface is a cylinder. Several parametrisations of such resonance surfaces for planar maps have been investigated in [32]. Our algorithm generalises a variant of one of these parametrisations to higher-dimensional maps; later in this section we adapt the same idea to the ODE case. See Section 5 for a discussion of potential limitations of this parametrisation for continuation.

We use the following typical example to illustrate both the circular topology of a constant α cross-section and the idea of our arc length parametrisation. Consider a family of invariant circles of a planar map for parameter values in the vicinity of a 1/2 Arnol′d tongue as depicted in Fig. 2, where we superimpose the (β, α) plane with the (β, x_1) plane to show the significance of the 1/2 Arnol′d tongue. However, we keep α constant as indicated with the constant-α line in the base plane of the figure. Now imagine a change of β along the constant-α line such that we cross the 1/2 tongue from left to right. The dynamics on the invariant circle is quasi-periodic or asymptotic to a high-periodic point for β outside but close to the tongue. For β on the boundary of the tongue, a period-two saddle-node bifurcation occurs and two period-two orbits are born on the invariant circle. Relative to the circle, one of these is stable (solid dots) and the other unstable (circles). As we continue to change β along the constant-α line, these two period-two orbits move along the invariant circle and collide with new partners in a period-two saddle-node bifurcation for β at the right-hand boundary of the 1/2 tongue. The path traced out by the period-two points in the full $\beta \times$ phase space is a smooth closed figure-eight curve, a closed curve (circular one-parameter family) of period-two orbits. We call this curve a constant-α cross-section.
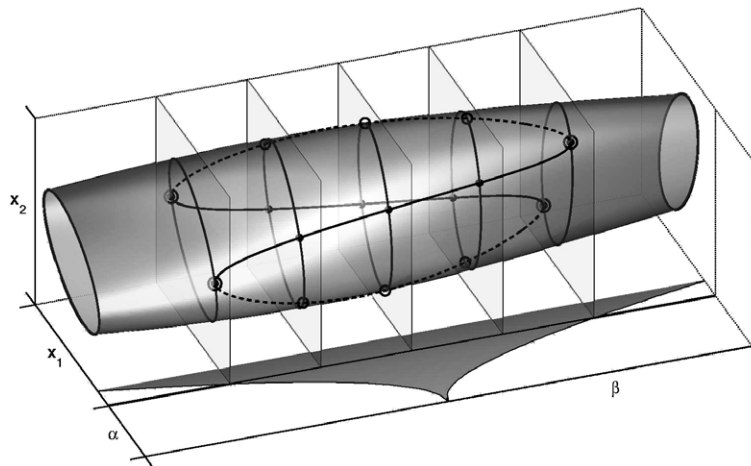

Fig. 2. A β-family of invariant circles of a planar map forms a tube in the (β, x_1, x_2)-space. A pair of period-two orbits exists on the invariant circle for β values within an Arnol′d tongue, one attracting (solid dots) and one repelling (circles). These orbits trace a smooth curve on the tube and appear and vanish in saddle-node bifurcations at the left and right boundary of the 1/2 tongue.

The (α, s) parametrisation of a resonance surface. If we introduce a suitable arc-length parametrisation for constant-α cross-sections as explained in the next two sections, then we can think of continuing this entire family of orbits with respect to the parameter α. Thereby, the constant-α cross-sections become closed coordinate lines on the resonance surface. We call this parametrisation of a resonance surface the "(α, s) parametrisation". In the actual computation we restrict the constant-α cross-sections to its fundamental domain by identifying permutations of the same orbit. We can assume that the number of mesh points required to approximate the fundamental domain with a certain accuracy stays constant as q increases. Hence, the dimension of our system of equations and the computation time will grow only linearly with q instead of being proportional to q^2.

The considerations above also explain why it is so hard to compute high-period Arnol'd tongues by fold continuation: the saddle-node bifurcations are the maxima and minima of β with respect to arc-length. With fold continuation one computes a locus of local extrema of a function that hardly varies if the tongue is very narrow. Especially as α approaches zero, the tongue widths approach zero, and β as a function of the arc length tends to a constant function.

2.1. Algorithm for maps

The above discussion leads to the following algorithm for computing the (α, s) parametrisation of a resonance surface; the boundaries of the Arnol'd tongue can then be obtained as the minima and maxima that β assumes. We set up a system of equations that uniquely determines a circular one-parameter family of periodic orbits. In the next subsection we replace the periodic orbit condition with a two-point boundary value problem to obtain a method for ODEs. We denote by $x^q := \{x_1^q, x_2^q, \ldots, x_q^q\} \in \mathbb{R}^{nq}$ the period-q orbit space and by $\xi = (x^q, a)$ an ordered pairing of a period-q orbit and a real number. We define the distance between two such pairs $\xi = (x^q, a)$ and $\eta = (y^q, b)$ in the "orbit cross parameter space" as

$$d(\xi, \eta) := \sqrt{\frac{1}{q} \sum_{i=1}^{q} \|x_i^q - y_i^q\|_2^2 + (a - b)^2}, \tag{3}$$

where $\|\cdot\|_2$ denotes the Euclidean norm in $\mathbb{R}^n$. A smooth closed curve of period-q orbits can now be represented as a periodic function $\xi(s) = (x^q(s), \beta(s))$, where s is the arc-length with respect to the distance d as defined in (3). We approximate the fundamental domain of such a closed curve by linear interpolation on N mesh points $\xi_j = (x_{\cdot j}^q, \beta_j)$, where $x_{\cdot j}^q$ refers to the full jth period-q orbit. If we demand that the mesh points are equally spaced with respect to the distance (3), then these points satisfy the following system of nonlinear equations

$$x_{1j}^q = f(x_{qj}^q, \alpha, \beta_j), \tag{4}$$

$$x_{2j}^q = f(x_{1j}^q, \alpha, \beta_j), \tag{5}$$

$$\vdots$$

$$x_{qj}^q = f(x_{q-1,j}^q, \alpha, \beta_j), \tag{6}$$

$$d(\xi_j, \xi_{j+1}) = h, \quad j = 1, \ldots, N-1, \tag{7}$$

$$d(\xi_N, \bar{\xi}_1) = h, \tag{8}$$

$$P(\xi) = 0, \tag{9}$$

where $j = 1, \ldots, N$ and $\bar{\xi} := (\{x_{\pi(1)}^q, x_{\pi(2)}^q, \ldots, x_{\pi(q)}^q\}, a)$ is the ordered pair with the one-shifted orbit of ξ. The cyclic permutation π is defined as $\pi(i) = i + \kappa$, where κ is the smallest natural number such that $p\kappa = \pm 1 \mod q$. The positive sign denotes a clockwise and the negative sign an anti-clockwise shift, in our implementation we use the clockwise shift. For example, for a 2/3 tongue we have $\bar{\xi}_1 = (\{x_{31}^3, x_{11}^3, x_{21}^3\}, a)$; see also Fig. 3.

The variable h denotes the unknown length of the line segments connecting two successive mesh points. Eqs. (4)–(9) form a system of $nqN + N + 1$ equations for the $nqN + N + 1 + 1$ unknowns x_{ij}^q, β_j, α and h. The "missing equation" is the arc-length condition automatically added by our continuation algorithm. The last equation $P(\xi) = 0$ is a scalar phase condition, which is necessary to fix the initial point ξ_1 on our
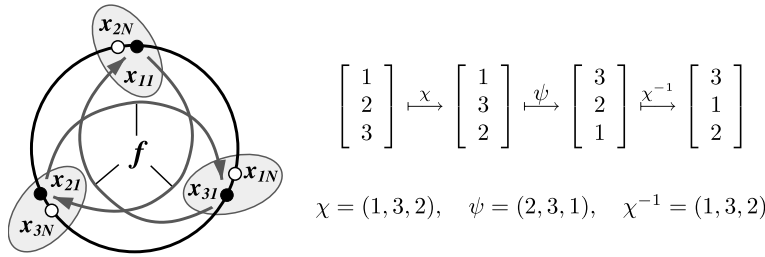
Fig. 3. The permutation π can be interpreted as a composition $\pi := \chi^{-1} \circ \psi \circ \chi$, where χ maps the dynamic order 1–2–3 of a 2/3 orbit to the geometric order 1–3–2, and ψ is the clockwise shift by one. The point x^3_{1N} approaches x^3_{31}, and so on. The dynamic order is assumed to be clockwise and the dynamics is indicated by the grey arrows with label f.

branch. A typical phase condition is the so-called Poincaré condition $x^q_{11,k} - c = 0$ for some suitable value of $k \in \{1, \ldots, n\}$ and $c \in \mathbb{R}$, that is, the kth component of the initial point of the orbit $j = 1$ is fixed to the value c. Note that the value p of a p/q Arnol'd tongue enters implicitly in condition (8) by means of the permutation π.

2.2. Algorithm for ODEs

To obtain an algorithm for Arnol'd tongues of an ODE, we have to replace the period-q orbit conditions (4)–(6) for maps by a suitable boundary value problem for periodic orbits of an ODE. The orbit space $\mathbb{R}^{qn}$ for maps is now replaced by the function space $\mathcal{X} := \{x_i : (0, 1) \to \mathbb{R}^n, i = 1, \ldots, q\}$ of segmented paths in the phase space. We do not explicitly require any smoothness of the paths, but if they satisfy the two-point boundary value problem in (11)–(14), they will automatically be smooth as well as periodic with period q. Analogous to the map case, we define a distance between two ordered pairs $\xi = (x, a)$ and $\eta = (y, b)$ in the orbit cross parameter space $\mathcal{X} \times \mathbb{R}$ as

$$d(\xi, \eta) := \sqrt{\frac{1}{q} \sum_{i=1}^{q} \int_{t=0}^{1} \|x_i(t) - y_i(t)\|_2^2 \, dt + (a - b)^2}. \tag{10}$$

A set of N mesh points $\xi_i = (x_i, \beta_i)$ on the fundamental domain of our family of periodic solutions is determined by the following system of equations.

$$\dot{x}_{ij} = T_{ij} f(x_{ij}, \alpha, \beta_j), \tag{11}$$
$$x_{1j}(0) = x_{qj}(1), \tag{12}$$
$$x_{2j}(0) = x_{1j}(1), \tag{13}$$
$$\vdots$$
$$x_{qj}(0) = x_{q-1,j}(1), \tag{14}$$
$$P_1(x) = 0, \tag{15}$$
$$d(\xi_j, \xi_{j+1}) = h, \quad j = 1, \ldots, N - 1, \tag{16}$$
$$d(\xi_N, \bar{\xi}_1) = h, \tag{17}$$
$$P_2(\xi) = 0. \tag{18}$$

The time-intervals for the segments $x_{ij}(t)$ have been rescaled to 1 and the values of the T_{ij} are the true time-intervals of the q segments $x_{ij}(t/T_{ij} - i + 1)$ of period-q solutions to the original ODE (2), and these T_{ij} can be different for each index i and j. Eqs. (11)–(14) are the boundary value problem for the qN n-dimensional unknowns x_{ij}, $i = 1, \ldots, q, j = 1, \ldots, N$. In our implementation we solve this boundary value problem by collocation. Eq. (15) is a set of qN scalar phase conditions fixing the initial points $x_{1j}(0), \ldots, x_{qj}(0)$ on the path segments. Eqs. (16)–(17) are also a set of N scalar equidistribution conditions. Eq. (18) is the same scalar condition as (9). The phase conditions (15) should be chosen carefully because the choice of initial points affects the distance between the periodic solutions $x_{\cdot j}$ in our metric, even though it does not affect the geometric paths

traced out by the periodic orbit in the phase space. A good condition seems to be to place all initial points $x_{1j}(0), \ldots, x_{qj}(0)$ in the same hyperplane. Together, Eqs. (15)–(18) specify $qN + N + 1$ equations for the $qN + N + 1 + 1$ parameters $T_{11}, \ldots, T_{qN}, \beta_1, \ldots, \beta_N, \alpha$ and h.

2.3. Convergence

The computation of a smooth family of periodic orbits as described in Sections 2.1 and 2.2 is an interpolation problem. We compute a piece-wise linear interpolation of the smooth "functions" $\xi(s) = (x^q(s), \beta(s))$ for maps and $\xi(s) = ([x(\cdot)](s), \beta(s))$ for ODEs. Since any smooth function can uniformly be approximated by a continuous piecewise linear function, Weierstraß' approximation theorem implies that the proposed method is uniformly convergent for $h \approx lN^{-1} \to 0$, where l is the total arc-length of the family. That $h = \mathcal{O}(N^{-1})$ is a basic result for continuously differentiable functions and the convergence is of order $\mathcal{O}(h^2)$ for two times continuously differentiable functions.

If we use piecewise linear interpolation, then the boundaries of an Arnol'd tongue are approximately given by $\min\{\beta_i\}$ and $\max\{\beta_i\}$. In this case we always have the inclusion $a \leqslant \min\{\beta_i\} \leqslant \max\{\beta_i\} \leqslant b$, where a and b denote the true left and right boundary. Note that the mesh points computed by our algorithm lie on the family within numerical accuracy, the arc-length condition merely serves as a distribution condition. Hence, we can also use higher-order interpolation in the arc-length for the functions ξ, for example, Fourier interpolation, as a post-processing step and compute the boundaries with high precision, but thereby possibly losing the inclusion property mentioned above.

2.4. Adaptation

The two algorithms (4)–(9) and (11)–(18) are suited for an intrinsic form of adaptation. Both systems contain a distribution condition, the arc-length conditions (7), (8) and (16), (17), respectively, which we can replace by a different one. In the present case, we follow the strategy of equidistribution of the interpolation error per line segment, which by standard interpolation theory is approximately proportional to $(\|\xi_i''\| + \|\xi_{i+1}''\|)h_i^2/16$, where ξ_i'' is the second derivative with respect to arc-length, $\|\xi_i''\| = d(0, \xi_i'')$ and h_i is the length of the line segment connecting the two consecutive mesh points ξ_i and ξ_{i+1}.

We have to take into account the situation that our solution curve may have segments that are (virtually) straight lines, that is, segments where $\|\xi''(s)\|$ is (almost) zero. Hence, an equidistribution with respect to the interpolation error could produce a mesh for which the distances $d(\xi_i, \xi_{i+1})$ do not uniformly tend to zero as N goes to infinity. In other words, we may lose convergence. To overcome this problem, we replaced (7), (8) and (16), (17) by the equidistribution condition

$$R_i(\xi) = r, \quad i = 1, \ldots, N,$$

where r is the value of the equidistributed error and the $R_i(\xi)$ are computed according to:

$$R_i(\xi) = \frac{h_i^2}{16}\left(\sqrt{(1-\sigma)^2 + \sigma\|\xi_i''\|_2^2} + \sqrt{(1-\sigma)^2 + \sigma\|\xi_{i+1}''\|_2^2}\right),$$

$$\xi_i'' = \frac{2}{h_i + h_{i-1}}\left(\frac{\xi_{i+1} - \xi_i}{h_i} - \frac{\xi_i - \xi_{i-1}}{h_{i-1}}\right),$$

$$h_i = d(\xi_i, \xi_{i+1}).$$

Here, the parameter $\sigma \in [0, 1]$ changes the behaviour of the adaptation. For $\sigma = 0$ we obtain the original distribution with constant step sizes h_i and for $\sigma = 1$ the interpolation error becomes equidistributed. Any other value of σ leads to a mixed strategy, which guarantees a uniform decrease of the step sizes h_i for $N \to \infty$ as well as a denser allocation of mesh points in regions with higher interpolation error. As an illustrative test example we computed the solution curve of the equation $(2x)^8 + y^8 = 1$ depicted in Fig. 4 using different values of σ. Apparently, the choice of $\sigma = 0.5$ seems to be a good compromise between full adaptation and a not too sparse overall distribution of mesh points.
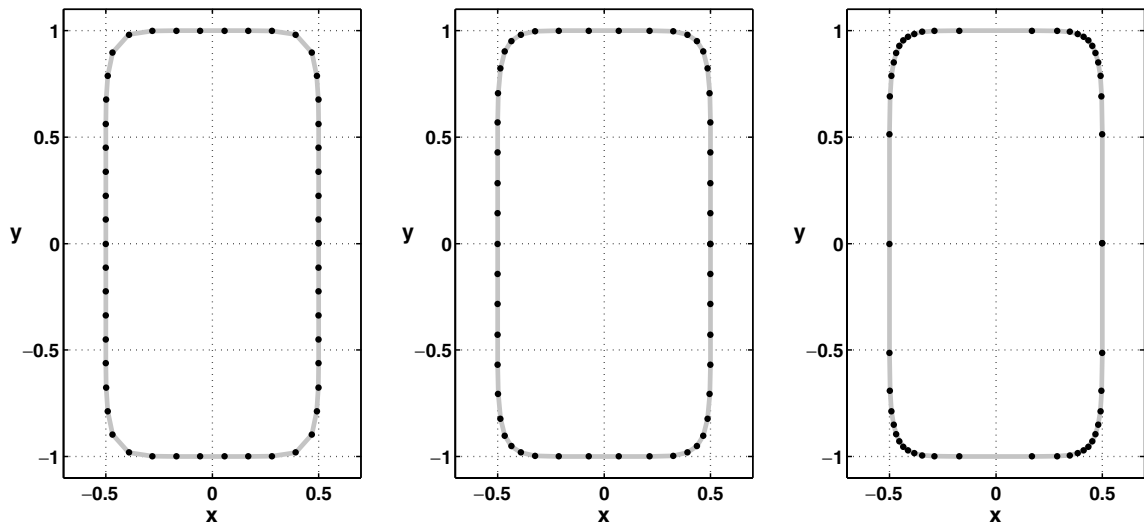
Fig. 4. Distribution of mesh points for the adaptation parameters $\sigma = 0$, 0.5, and 1.0 (from left to right) for the test example $(2x)^8 + y^8 = 1$.

3. Computation of quasi-periodic arcs

A variety of algorithms for the computation of invariant circles of maps have been proposed, some use a suitably generalised Poincaré map [23,24], some are based on "ad-hoc" parametrisations [9,13,15,25,30,38] and others involve the Denjoy parametrisation explained below; see [10,11,19,20,22]. We use a method based on the Denjoy parametrisation for two reasons: this parametrisation is unique up to a phase shift, which leads to a particularly simple algorithm; see also [36]. Furthermore, it contains the rotation number explicitly. The latter property is a prerequisite for applying Newton's method, because the rotation number is not a differentiable function of the two parameters α and β. Hence, a condition like $\mathrm{rot}(\alpha, \beta) = \varrho$ would effectively prevent the use of Newton's method.

The methods for maps in [10,19,20,22] have also been used to compute tori of ODEs by replacing the map with the solution of an initial value problem. For completeness, we briefly review these methods for one-dimensional tori, that is, for invariant circles, and show how to replace the invariance condition for maps by a two-point boundary value problem that can be solved with the method of collocation. Note that this approach is different from the initial value problem technique mentioned above, which leads to a single-shooting method that is known to be ill-posed in many cases, in particular, for stiff equations. In what follows, the term "torus" always refers to either an invariant circle of a map or an invariant two-torus of an ODE.

A quasi-periodic invariant circle with fixed irrational rotation number ϱ of the map (1), $x \mapsto f(x, \alpha, \beta)$, is a solution of the invariance equation $u(\theta + 2\pi\varrho) = f(u(\theta), \alpha, \beta)$. That is, the map restricted to the invariant circle $\{u(\theta)|\theta \in [0, 2\pi]\}$ is conjugate to a rigid rotation with rotation number ϱ. We approximate u by a Fourier polynomial of order N, that is, $u_N(\theta) = \sum_{k=-N}^{N} c_k e^{jk\theta}$, where θ lies on the unit circle parametrised over $(-\pi, \pi]$ and j denotes the imaginary unit. We compute the coefficients c_k by collocation, that is, we introduce a uniform mesh $\theta_k = (k + 1)\pi/(N + 1)$, $k = -N, \ldots, N$, on the unit sphere and require that the invariance condition holds on the mesh points. This leads us to the system of nonlinear equations

$$u_N(\theta_k + 2\pi\varrho) = f(u_N(\theta_k), \alpha, \beta), \tag{19}$$
$$P(u_N) = 0, \tag{20}$$

where (20) is again a scalar phase condition. This are $n(2N + 1) + 1$ equations for the $n(2N + 1)$ unknown Fourier-coefficient vectors c_k and the two parameters α and β. Note that we implicitly exploited that $c_{-k} = \bar{c}_k$ in this count.

It is essential for this approach that the irrational rotation number is kept constant. In that case the continuation follows a smooth quasi-periodic arc in the parameter plane. If one would use system (19), (20) to perform a one-parameter continuation with ϱ taken as a variable and either α or β fixed, then this path would intersect Arnol′d tongues. Hence, the rotation number assumes rational values on an open and dense set along this path. This leads to a failure of the algorithm because the Denjoy parametrisation exists only for invariant circles with irrational rotation number; see [36] for example computations illustrating this effect.

The invariance condition (19) for maps can be replaced by the two-point boundary value problem

$$\dot{x}_k = Tf(x_k, \alpha, \beta), \tag{21}$$
$$x_k(0) = u_N(\theta_k), \tag{22}$$
$$x_k(1) = u_N(\theta_k + 2\pi\varrho), \tag{23}$$
$$P_1(x) = 0, \tag{24}$$
$$P_2(u_N) = 0, \tag{25}$$

for computing an invariant torus of the ODE (1), $\dot{x} = f(x, \alpha, \beta)$. The variable T is the common return time of all the solutions x_k. Eq. (25) is the same scalar condition as (20) and condition (24) is a scalar phase condition to fix an initial point on some solution of the set $x = \{x_{-N}, \ldots, x_N\}$. Together, Eqs. (21)–(23) are a $2n(N+1)$-dimensional boundary value problem for the $2N+1$ n-dimensional unknown functions $x_{-N}(t), \ldots, x_N(t)$ and the $2N+1$ Fourier coefficient vectors $c_{-N}, \ldots, c_N$. Eqs. (24)–(25) specify two conditions for the three parameters T, α, and β. Note that we omitted the trivial ODEs $\dot{c}_k = 0$ that need to be included in (21)–(23) if one wants to use standard continuation software for boundary value problems such as AUTO [16].

4. Examples

In this section, we consider three examples: an embedded Arnol′d family in Section 4.1, a generic caricature example in Section 4.2 and a system of two linearly coupled Van der Pol oscillators in Section 4.3; see also Section 1. For all three examples we compute a large set of Arnol′d tongues and companion quasi-periodic arcs. The embedded Arnol′d family is a two-dimensional map that has the unit circle as a global attractor and its restriction to the unit circle is the well-known Arnol′d family $x \mapsto x + \varrho + a\sin 2\pi x \pmod 1$. The generic caricature family was studied in the prior papers [27,28,31,32] by computing resonance surfaces and their projections to Arnold tongues. We compute here a much larger set of Arnol′d tongues, using the algorithms presented in this paper, and, for the first time, the companion quasi-periodic arcs. The system of two linearly coupled Van der Pol oscillators is a classic example of an ODE showing quasi-periodic behaviour and phase-locking; see, for example [17,34]. As explained in Section 1, the computation of high-period Arnol′d tongues is particularly difficult for this system and our computation of a large set of Arnol′d tongues demonstrates the success of our generalisation of the methods for planar maps discussed in [32]. All three examples have two parameters α and β, where α is a coupling strength and β controls the rotation number or the natural frequencies of the system.

To automate our computations we use two algorithms that produce sets of rotation numbers for which we subsequently compute the Arnol′d tongues and quasi-periodic arcs. The user needs only to specify the "level" of rotation numbers for each of these two computations, which are then performed in two loops in a single computer program. The choice of rotation numbers for Arnol′d tongues is straightforward using a so-called Farey sequence of level l. We start with the sequence $L_0 = \{0/1, 1/1\}$ and compute the sequence L_{k+1} by inserting all Farey sums of successive rationals of L_k into the sequence L_k, where the so-called Farey sum is defined as $o/p \oplus q/r := (o+q)/(p+r)$. We obtain increasingly larger sets of rational numbers, the Farey sequences $L_1 = \{0/1, 1/2, 1/1\}$, $L_2 = \{0/1, 1/3, 1/2, 2/3, 1/1\}$, $L_3 = \{0/1, 1/4, 1/3, 2/5, 1/2, 3/5, 2/3, 3/4, 1/1\}$, and so on. Starting with L_0 as above, it is guaranteed that all the fractions are reduced, any rational number is a member of some sequence, the sequences are ordered and the denominator increases with the level l.

It is much more delicate to choose "as irrational as possible" rotation numbers for the continuation of quasi-periodic invariant tori, because we cannot represent true irrationals as floating point numbers. We used two sequences, the golden mean sequence and the symmetric golden mean sequence, that both worked well in our examples. We start with the sequence $G_0 = \{0, 1\}$ and compute the sequence G_{k+1} by inserting all golden

mean subdivisions $x + g(y - x)$ of successive elements x and y of G_k into the set G_k, where $g = 2/(1 + \sqrt{5}) \approx 0.6180\ldots$ We obtain the sequence of larger and larger sets $G_1 = \{0, g, 1\}$, $G_2 = \{0, g^2, g, 3g - 1, 1\}$, and so on. Note that these sets contain the noble sequence $\{g, g^2, g^3, \ldots\}$ as a sub-sequence. The symmetric golden mean sequences are computed in the same way, except that we insert the two subdivisions $y - g(y - x)$ and $x + g(y - x)$. Both sequences eventually contain the same rotation numbers, but we preferred the symmetric variant for problems with some symmetry with respect to the rotation number $\varrho = 1/2$, such as the embedded Arnol'd family.

The construction of initial solutions is straightforward for the embedded Arnol'd family and the caricature example. For $\alpha = 0$ both maps have the unit circle as an attracting invariant circle and the maps restricted to this circle reduce to a rigid rotation for any parameter β. Obtaining initial solutions for the system of two coupled Van der Pol oscillators is more involved. For $\alpha = 0$ the two oscillators decouple and the first one has a limit cycle that is independent of β and can be approximated by a Fourier polynomial. We computed a β-dependent Fourier approximation for the β-family of limit cycles of the second oscillator. With these two approximations at hand, we can construct approximate initial solutions for the boundary value problems (11)–(18) and (21)–(25) by superposition. We used the Poincaré condition $\dot{y} = 0$ and all T_{ij} were initially set to T/q, where T is the period of the second oscillator. This initial approximation needs to be corrected by Newton's method before starting the actual continuation with respect to α.

For all three examples the continuation of quasi-periodic invariant tori does not cause any problems. The arc-length continuation of families of such tori is well defined as long as the quasi-periodic tori persist. We compute curves of tori whose projections to the parameter plane are always one-dimensional. Difficulties arise in the computation of resonance surfaces, because here the solution to our equations may cease to exist during continuation due to geometric reasons. The arc-length continuation of constant-α cross-sections relies on the fact that these sections are continuously changing single closed curves. The failure of this cross-sectional assumption is illustrated with the caricature map example. This observation suggests that one might want to use our algorithm for Arnol'd tongues just for branch-switching from zero forcing or decoupling $\alpha = 0$, that is, to compute only the tips of the tongues and switch to fold continuation as soon as the variation in the parameter β permits it. However, our implementation is designed to proceed as far as possible and the examples demonstrate that we are, in many cases, able to compute the entire resonance surface, and particularly the p/q resonance surfaces for $q \geqslant 5$.

4.1. The embedded Arnol'd family

Our first example is the classic text book example of the Arnol'd family

$$x \mapsto x + \varrho + a \sin 2\pi x \pmod 1.$$

See, for example [1,4,14,17,21]. To get rid of the modulus, we rewrite the Arnol'd family as a map acting on the unit circle $r = 1$ in polar coordinates. We identify $2\pi x$ with the angle θ, which leads to the two-dimensional map

$$\theta \mapsto \theta + 2\pi\beta + \alpha \sin \theta, \tag{26}$$
$$r \mapsto 1. \tag{27}$$

For the actual computations we used the composite map $f := \psi \circ g \circ \psi^{-1}$, the embedded Arnol'd family, where g is the map defined by Eqs. (26), (27) and ψ is the transformation of polar into Cartesian coordinates. For a and ϱ we have the relations $\varrho = \beta$ and $2\pi a = \alpha$.

For completeness and comparison we state here some well-known results of circle-map theory about the Arnol'd family; see also [2,3,14,17,21]. We restrict the map (26)–(27) to the invariant circle $r = 1$, that is, we consider only the map (26). Furthermore, we denote the set of rotation numbers depending on α and β with $\varrho_{\alpha\beta}$. The rotation number is unique for $0 \leqslant \alpha \leqslant 1$ and a closed interval for $\alpha > 1$ [4]. The map (26) is diffeomorphic for $0 \leqslant \alpha < 1$, homeomorphic for $\alpha = 1$ and non-invertible for $\alpha > 1$. The line $\alpha = 1$ is called the critical line. For $\alpha = 0$ the map becomes a rigid rotation with rotation number $\varrho_{0\beta} = \beta$. That is, if $\beta = p/q$

is rational, then every orbit is q-periodic, and if β is irrational, then every orbit is quasi-periodic and dense on the circle.

Each point on the line $\alpha = 0$ for which $\beta = p/q$ is rational is the tip of a p/q-Arnol'd tongue, which have the shape of a wedge that opens up for increasing α; see also the left-hand panel in Fig. 5. The tongues have non-zero width, but do not overlap for $0 < \alpha \leqslant 1$, and the union of all tongues is an open-dense set in the parameter plane. The width of the Arnol'd tongues decreases rapidly as the period q increases. For parameter values in a p/q Arnol'd tongue, all orbits under (26) are asymptotic to a q-periodic orbit. From each point on the line $\alpha = 0$ for which β is irrational, a quasi-periodic arc emanates. These arcs sit in between the Arnol'd tongues and continue up to $\alpha = 1$. The orbits under (26) are quasi-periodic and dense on the circle, and the map is conjugate to a rigid rotation with rotation number $\varrho_{0\beta} = \beta$ for parameter values along such an arc. The conjugacy is for $\alpha < 1$ analytic, if this rotation number is Diophantine and of finite smoothness otherwise. Irrational numbers that are *not* Diophantine are called *Liouville* numbers. The set of Liouville numbers in $[0,1]$ is dense, but has zero measure. The conjugacy with a rigid rotation loses its smoothness as the critical line $\alpha = 1$ is approached. The intersections of the quasi-periodic arcs with horizontal lines $\alpha = \text{const.}$ form a family C_α of Cantor sets that have positive measure for $0 \leqslant \alpha < 1$. In particular, we have $\mu(C_0) = 1$ and $\mu(C_\alpha) \to 0$ as $\alpha \to 1$. For $\alpha > 1$, the maps are no longer homeomorphisms, and therefore not conjugate to an irrational rotation [4]. Consequently, our algorithm, which actually solves for a conjugacy with the irrational rotation, fails beyond $\alpha = 1$.

Arnold tongues. The results of our numerical computations are shown in the left-hand panel of Fig. 5. We computed the Arnol'd tongues for the rotation numbers in the Farey sequence L_5 and the quasi-periodic arcs for the rotation numbers in the symmetric golden mean sequence $G_2 \backslash \{0,1\}$. Our computations accurately reproduce the results of circle-map theory stated above. The uniform convergence of the method for Arnol'd tongues is illustrated in the right-hand panel of Fig. 5. By definition of the map, the projection of any resonance surface of the embedded Arnol'd family to the phase plane is the unit circle, and its constant α cross-sections of resonance surfaces are cylinders for all values of α, even if $\alpha > 1$. Therefore, the (α, s) parametrisation is globally defined and it is not a problem to compute even larger sets of Arnol'd tongues than the ones shown in Fig. 5.

The sequence of four pictures in Fig. 6 exemplifies part of the geometric structure of the 1/4 resonance surface. The top-left-hand panel shows its projection to the parameter plane, which forms the 1/4 Arnol'd tongue. In the other three figures we gradually rotate the surface in the (α, β, x_1)-space and the typical period-four saddle-node structure becomes visible. The colouring of the surface is proportional to the deviation of β from its average value in the corresponding constant-α cross-section and was added for comparison with Fig. 7.
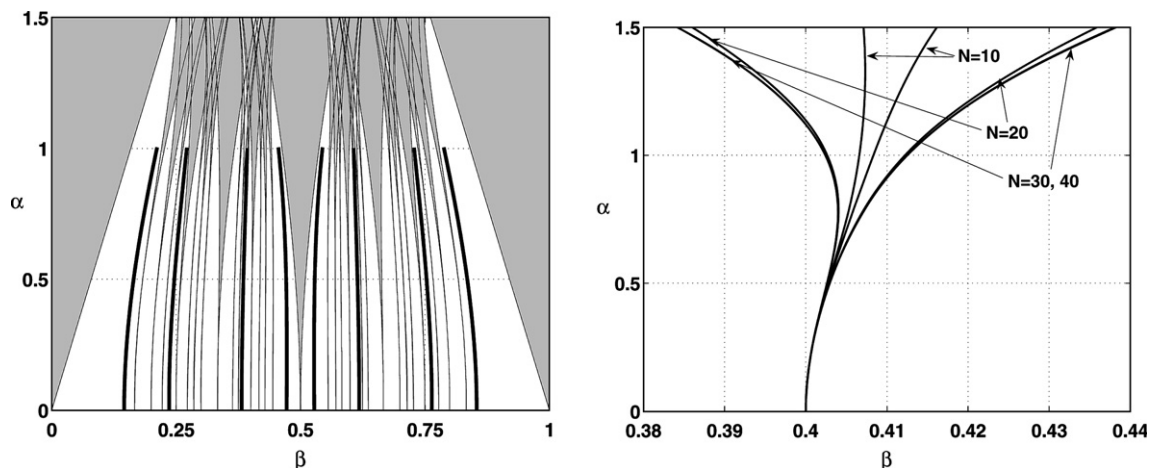

Fig. 5. The left-hand panel shows the Arnol'd tongues for the rotation numbers in the Farey sequence L_5 (grey shaded) and quasi-periodic arcs for the rotation numbers in the symmetric golden mean sequence $G_2 \backslash \{0,1\}$ (thick black) of the embedded Arnol'd family. The uniform convergence of our method is illustrated with the boundaries of the 2/5 tongue in the right-hand panel for the adaptation parameter $\sigma = 0.5$ and $N = 10, 20, 30$ and 40 mesh points. The boundaries for $N = 30$ and $N = 40$ are practically on top of each other.
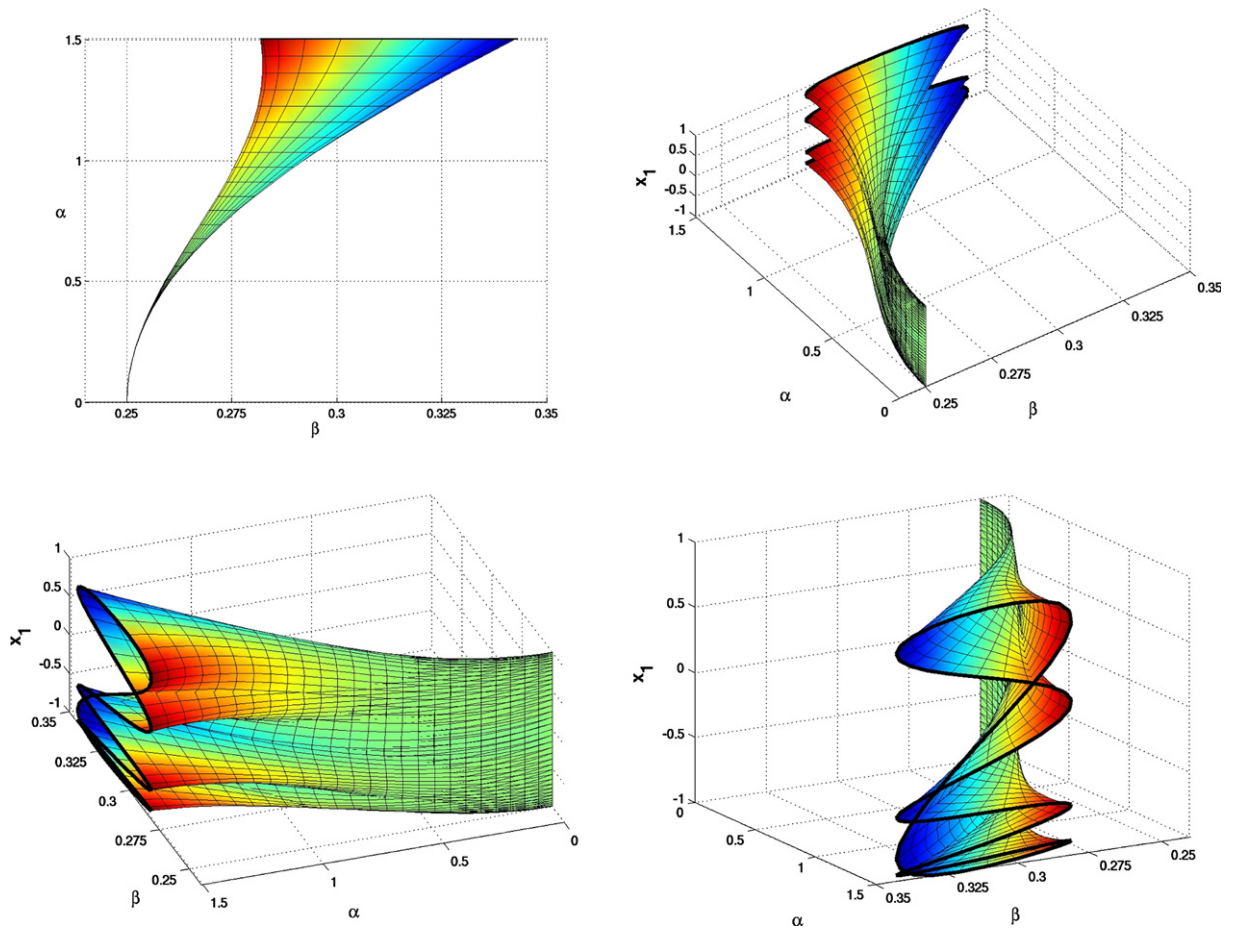
Fig. 6. Different projections of the 1/4 resonance surface of the embedded Arnol'd family. The projection onto the (β, α)-parameter plane is the 1/4 Arnol'd tongue (top left). In the other figures we added the coordinate x_1. The colouring for fixed α is relative to the average value of β and gives an impression of the variation of β.
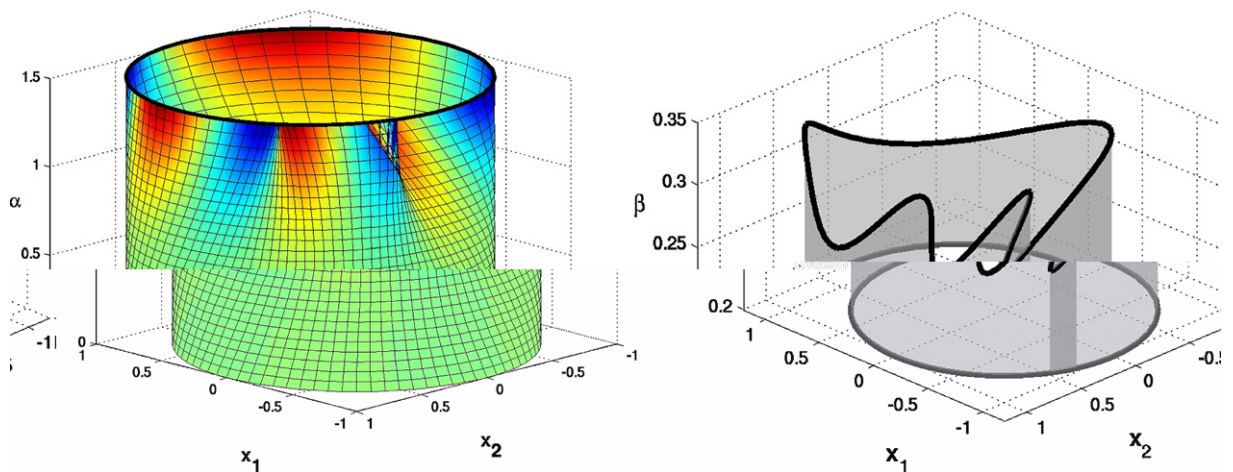

Fig. 7. The 1/4 resonance surface projected onto the (x_1, x_2, α)-space (left). The colouring is as in Fig. 6 and gives an impression of the variation of the surface in the fourth dimension β. In this projection the resonance surface becomes multi-valued for $\alpha > 1$. This is clearly illustrated in the right-hand figure, where the $\alpha = 1.5$ family is depicted together with the shadow it casts onto the (x_1, x_2) plane. Compare this view of the curve with the front edge of the surface in the lower-right picture in Fig. 6 – another view of the same curve.

We visualise the full four-dimensional geometry of the 1/4 resonance surface in the left-hand panel of Fig. 7. The projection of the resonance surface onto the (x_1, x_2, α)-space is a cylinder with radius one. The colouring is as in Fig. 6 and is proportional to its relative variation in the fourth dimension β. The self-intersection for $\alpha > 1$ is due to projection. This is made clear in the right-hand panel of Fig. 7 where the constant-α cross-section of the resonance surface for $\alpha = 1.5$ is shown in the (x_1, x_2, β)-space. The vertical projection of this curve onto the (x_1, x_2)-plane is the unit circle and the curve overlaps itself in this vertical projection, which is indicated by the darker shadow that a fold-like structure casts.

The embedding of the Arnol'd family was solely introduced to eliminate a modulo operation. Hence, one can reduce the dimension of the embedding space of the resonance surfaces by omitting the trivial coordinate $r = 1$. This would allow us to visualise the full geometry of these resonance surfaces in a three-dimensional space. See a related study in [29].

Quasi-periodic arcs. From the results of our computations of quasi-periodic arcs we can produce an approximation of the conjugacy under which the map (26) becomes a rigid rotation. Condition (19) can be read as $f \circ u = u \circ R_\varrho$. In other words, our algorithm computes an approximation to the inverse of a conjugacy under which the map f restricted to its invariant circle γ becomes a rigid rotation, that is, $h \circ f = R_\varrho \circ h$ with $h = (u|_\gamma)^{-1}$. The graphs of the conjugacy h for the golden mean rotation number and different values of α are shown in Fig. 8 as black curves. The top two panels show this conjugacy for moderate values of α and the bottom four panels show it for a sequence of α values that closely approach the critical line where a loss of smoothness occurs. We plotted the graphs of the derivatives of h as grey curves in logarithmic scale and they indeed seem to reflect this loss of smoothness. However, one has to exercise some care when interpreting these figures, in particular, the bottom two panels. In our case we need to check if and in what sense our method converged to a solution of the invariance condition (19). For our computations we used Fourier polynomials of increasing orders N that are powers of two. The graphs are shown for $N = 512$, which was the highest such order for that our Fourier polynomial for $\alpha = 0.9999$ produced an invertible h. It seems that we reached the accuracy limit of double precision arithmetic at this point.

To check convergence we computed the five different measures of approximation errors that are shown in Table 1. Let us, for brevity, denote the l_2-norm of the Fourier coefficients of a Fourier polynomial u_N by $R(u_N)$ and the l_2-norm of the second half of the coefficients, that is, for $|k| = N/2, \ldots, N$, by $r(u_N)$. Then, the columns in Table 1 show from left to right the parameter α, the absolute error $r(u_N)$ of u_N, the relative error $r(u_N)/R(u_N)$, the absolute error $r(u_N')$ of the derivative $u_N' = du_N/d\theta$, the relative error $r(u_N')/R(u_N')$ and the logarithm of $r(u_N')$. The error measures for u_N in columns AE and RE indicate that the solution u_N and, thus, the conjugacies h are reasonably well approximated. The Fourier coefficients decay sufficiently fast and the second halves of the Fourier coefficients add up to at most 12% of the norm of u_N (column AE). This picture changes if we look at the derivative u_N'. The relative error (column RED) in the last two rows is greater than 50%, that is, there is no indication of decay. The absolute error of $dh/d\phi$ is at least of the same order of magnitude as the absolute error of u_N' (column AED). Hence, the error in $dh/d\phi$ might be as large as the function values of $dh/d\phi$, which means that the graphs of $dh/d\phi$ in the bottom two panels of Fig. 8 are by no means reliable. However, this "loss of convergence" in the derivative is in itself an indicator of a loss of smoothness for $\alpha \to 1$.

4.2. A generic caricature example

Our second example is a two-parameter family of maps of the plane that is constructed to mimic the behaviour of the Poincare return map of a periodically forced oscillator. Alternatively, this caricature map can be thought of as a periodically forced oscillator with "impulse forcing" by composing the time-one flow of an autonomous flow in the plane with a map that provides a periodic "kick" to the solution. The kick is defined as the identity for $\alpha = 0$ and increasing in magnitude as α increases. More specifically, this map is defined as

$$H_{(\beta,\alpha)} := g_\alpha \circ h_\beta,$$

where $h_\beta(x)$ is the time-one map of the following differential equation, given in polar coordinates:

$$\dot{r} = \frac{r(1 - r^2)}{1 + r^2}, \quad \dot{\theta} = 2\pi\beta + \frac{1 - r^2}{1 + r^2},$$
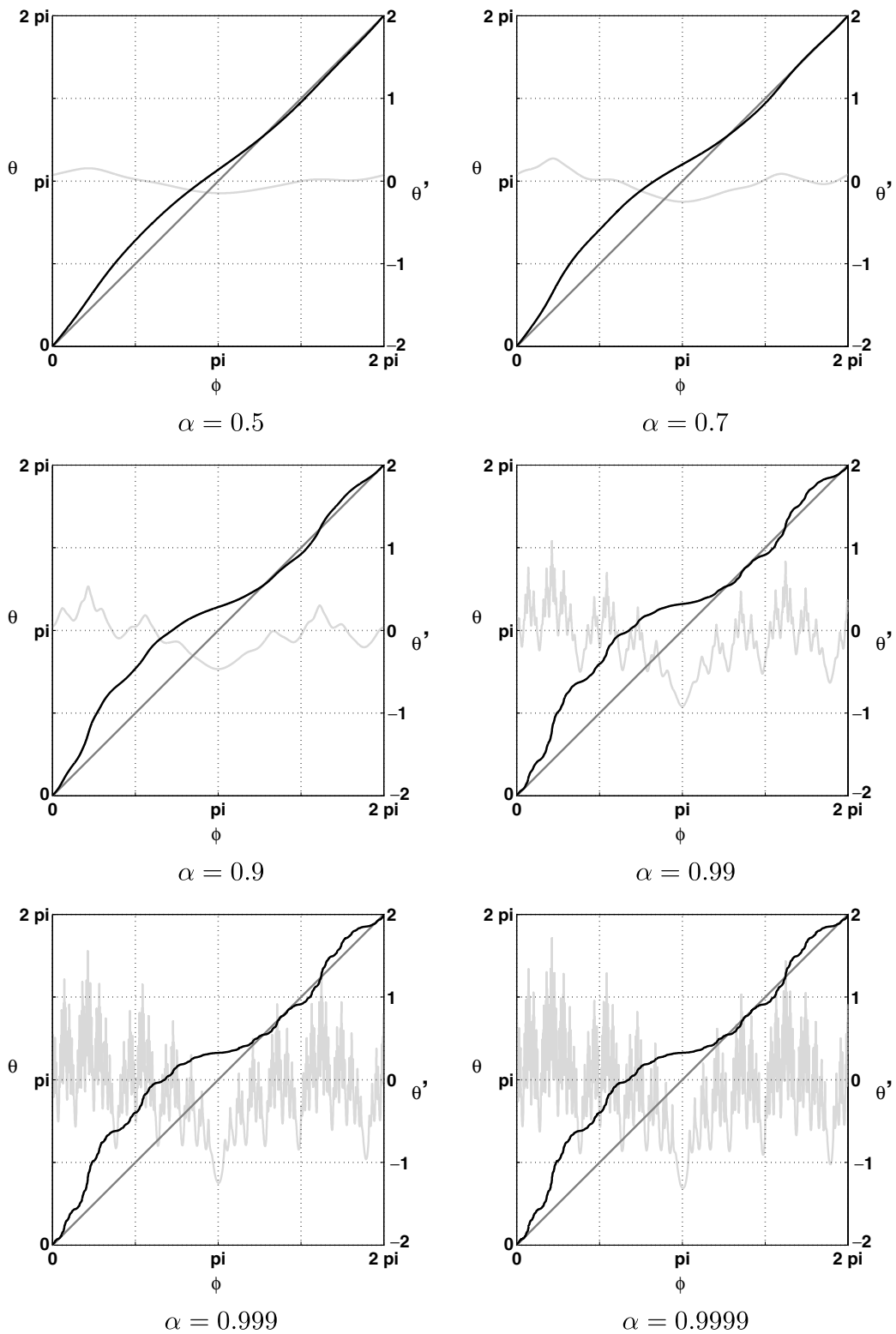
Fig. 8. Graphs of the conjugacy $\theta = h(\phi)$ (black curves) for different values of α under which the embedded Arnol′d family becomes a rigid rotation with golden mean rotation number. We used $N = 512$ Fourier modes to compute these figures. The dark diagonal line is the graph of the identity and the light grey curves show the logarithm of the derivative $\theta' = d\theta/d\phi = dh/d\phi$.

Table 1
Estimated errors for the golden invariant circle approximated with $N = 512$ Fourier modes for different values of α

α	AE	RE	AED	RED	LAED
0.5000	8.1841e − 07	1.4159e − 07	1.4792e − 05	2.5039e − 06	−4.83
0.7000	1.0475e − 06	1.6781e − 07	1.7399e − 05	2.5654e − 06	−4.76
0.9000	1.0822e − 04	1.5760e − 05	1.2783e − 03	1.4428e − 04	−2.89
0.9900	3.0418e − 01	4.0791e − 02	3.9073e + 00	2.5855e − 01	0.59
0.9990	8.2456e − 01	1.0782e − 01	1.1407e + 01	5.3253e − 01	1.06
0.9999	9.1878e − 01	1.1966e − 01	1.2907e + 01	5.6515e − 01	1.11

The columns from left to right show α, the absolute and relative error of the solution and the absolute, the relative and the logarithm of the absolute error of the derivative of the solution.

and g_α is the map

$$(x_1, x_2) \mapsto (1 - \alpha)(x_1 - 1, x_2) + (1, 0).$$

Note that in this setup, β is not restricted to be positive, but is allowed to be any real number. So our parameter space is $\mu = (\beta, \alpha) \in \mathbb{R} \times [0, 1)$.

For $\alpha = 0$ the unit circle is invariant and attracting. The restriction of the caricature map to this circle is a rigid rotation with rotation number β (mod 1). The invariant circle persists for sufficiently small forcing $\alpha > 0$, but the dynamics on the circle will change according to the Arnol′d tongue scenario; see also Section 4.1. Arnol′d tongues emanate from the line $\alpha = 0$ with their tips at points where β is rational, and quasi-periodic arcs start at points for which β is an irrational. The left-hand panel of Fig. 9 shows the Arnol′d tongues for the rotation numbers in the Farey sequence L_6, and the right-hand panel the quasi-periodic arcs for the rotation numbers in the symmetric golden mean sequence $G_3 \backslash \{0, 1\}$.

To elaborate somewhat, we note that an oversimplified but useful crude description of the dynamics in the caricature family is that the invariant circle that exists at $\alpha = 0$ shrinks in size as α increases, and the rotation of the phase space increases as β increases. For large enough α, any invariant circle or periodic orbit has disappeared, leaving only a globally attracting fixed point. This bifurcation generally happens along a Neimark–Sacker curve (dashed black curve). This suggests that both the surface of invariant circles in the phase cross parameter space corresponding to a continuation of an irrational arc, and the resonance surfaces corresponding to the continuation of a tongue, are topological disks. This is corroborated in Fig. 10; see also [28,32].
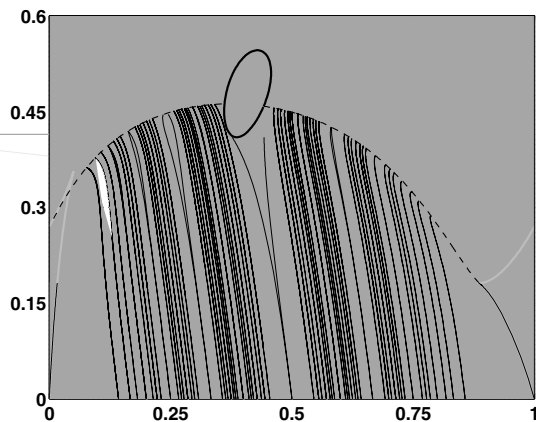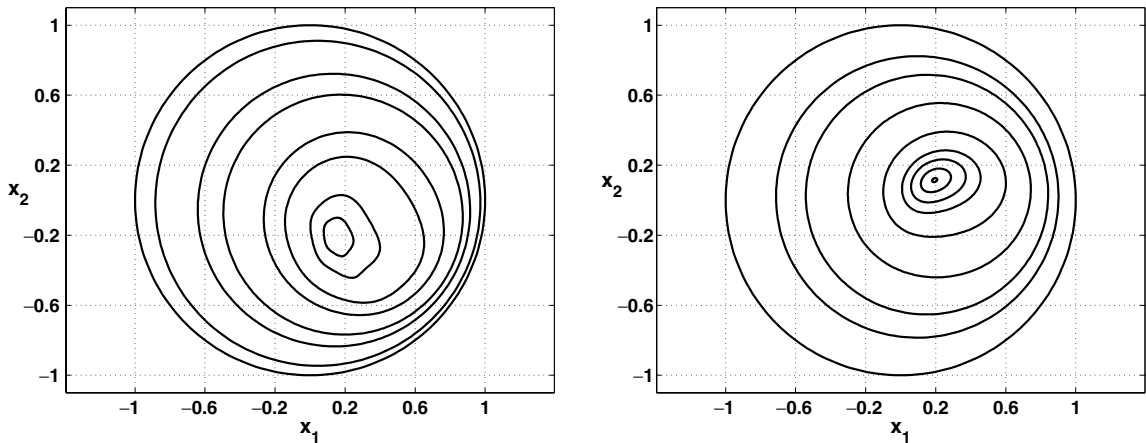
Fig. 10. Some constant-α cross-sections of the 1/5 Arnol'd tongue projected to the phase space (left) and golden invariant circles (right) of the caricature family. These cross-sections and circles collapse for increasing α to a fixed point on a Neimark–Sacker bifurcation curve.

Exceptions are the period-two surfaces, which are Möbius strips, and the period-one surface, which is unbounded since it is in the same fixed-point component as the repelling fixed point that continues from the origin for the unforced oscillator.

The tongues in Fig. 9, connecting zero forcing amplitude to the Neimark–Sacker curve, provide a comparison of the two Arnold tongue scenarios. We have been describing the local situation near zero forcing in this paper. The closed curve of periodic orbits corresponding to a cross-section of a tongue near a Neimark–Sacker curve is topologically the same as the cross-sections we have been computing and continuing from zero forcing amplitude. The difference is that the closed curve shrinks to a point at the Neimark–Sacker curve, while it remains as a "large" topological circle at the zero forcing point. This suggests that our algorithm could be adapted to continuation from Neimark–Sacker curves as well. We hope to pursue this in the future. Also different in the two scenarios are the widths of the projections to the tongues in the parameter plane. The Neimark–Sacker tongue boundaries have a tangency of order $(q - 2)/2$ [1,26,33,37], whereas the zero forcing amplitude tongues have a nonzero opening angle [18]. Furthermore, the case of strong resonances (periods $1, 2, 3, 4$) is distinct in the Neimark–Sacker case [1,26,37].

Continuations of the arcs and tongues terminated for a variety of reasons, some because the complete resonance surface had been computed, and others due to limitations of our algorithm. Continuations that reach the fixed point on the Neimark–Sacker curve in either of the two cases are complete; the global arc/tongue has been computed. A close inspection of the quasi-periodic arcs' approach to the Neimark–Sacker curve in the right-hand part of Fig. 9 reveals that the arcs cross the Neimark–Sacker curve and turn to the right to finally arrive at the Neimark–Sacker curve from above. This is due to a "Chenciner point" on the Neimark–Sacker curve, at approximately $(\beta, \alpha) = (0.75, 0.3)$, where the bifurcations change from supercritical to subcritical and the arcs/tongues change from approaching the Neimark–Sacker curve from below to approaching from above [12]. This poses no difficulties to arc-length continuation of the quasi-periodic arcs, which are all completely computed. For the tongues, however, we make an additional cross-sectional assumption that fails to hold in this and other situations. We require that the constant-α cross-section is circular, but in the region where the tongues "bend back" we have a more complicated merging of two such circular sections, which is not representable as a solution of our Eqs. (4)–(9); see Fig. 11.
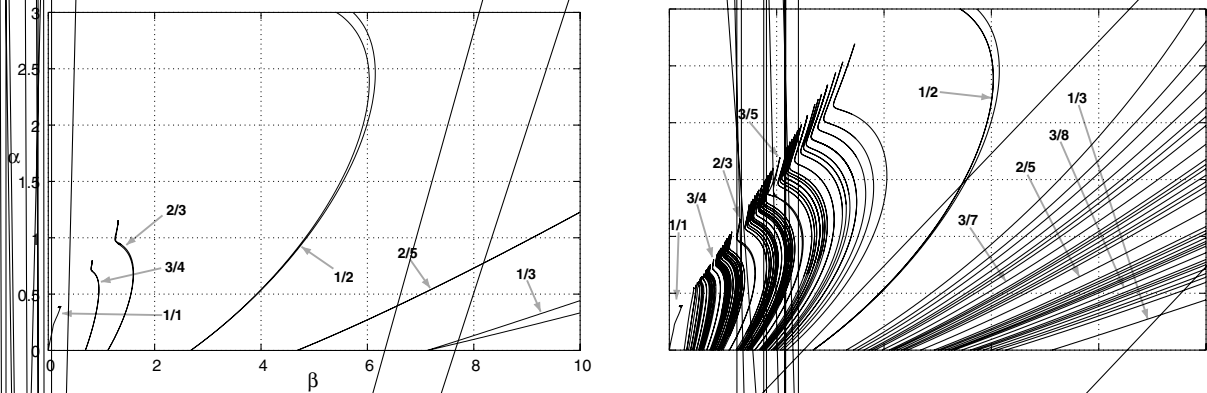
The continuations that failed to be complete did so because the constant-α cross-sections ceased to be topological circles at some value of α. These failures included the tongues toward the right-hand edge of the Neimark–Sacker curve which turn around and are headed down (in the (β, α) plane) as they approach the Neimark–Sacker curve, and the strongly resonant cases that are pictured in Fig. 12. See [32] for alternative parametrisations of resonance surfaces which do allow complete computation of tongues for the caricature map.

4.3. Two coupled Van der Pol oscillators

As our final example we return to the system of two linearly coupled Van der Pol oscillators,

$$\ddot{x} + \varepsilon(x^2 - 1)\dot{x} + x = \alpha(y - x),$$
$$\ddot{y} + \varepsilon(y^2 - 1)\dot{y} + (1 + \beta)y = \alpha(x - y),$$

which we introduced at the beginning of this paper; see also [17,34,36]. The parameter ε changes the non-linear damping in the system, α is the coupling strength and β is a detuning parameter that controls the natural frequency of the second oscillator. The oscillators decouple for $\alpha = 0$ and their product is a normally attracting invariant torus. This torus will survive for sufficiently small coupling strength and the two oscillators either synchronise (phase-lock) or oscillate independently with incommensurate internal frequencies. Hence, we have Arnol'd tongues and quasi-periodic arcs emanating from the decoupling line $\alpha = 0$. For large enough α one of the internal frequencies becomes suppressed in an inverse Neimark–Sacker bifurcation where the torus col-

and allows the computation of large sets of Arnol′d tongues, including their tips. In the right-hand panel of Fig. 13 we observe the typical distribution of Arnol′d tongues that is induced by the self-similarity of Devil's staircase [14,21]; see also the left-hand panel in Fig. 9. Close to the strong resonances we find large regions in parameter space for which we have predominantly quasi-periodic or desynchronised states, that is, the quasi-periodic arcs cover a set with large relative measure.

Since the Arnol′d tongues connect to a locus of Neimark–Sacker bifurcations (not shown), we experience difficulties computing the resonance surfaces of the strong resonances because they are not cylindrical close to the Neimark–Sacker curve; see Section 4.2 for more details. However, except possibly for the tips near the line $\alpha = 0$, the boundaries of these tongues can be computed by fold continuation; compare the boundaries of the 1/1 tongue in Fig. 1 and in the left-hand panel of Fig. 13. Combining both techniques we can obtain the complete picture.

5. Discussion and outlook

The computation of quasi-periodic invariant tori is a problem for which well-tested algorithms were already available for some time [10,22], and a two-parameter continuation of quasi-periodic invariant tori was proposed in [36]. The specific application of the algorithm [10,22] to form a two-point boundary value problem for quasi-periodic tori of ODEs as described in Section 3 is new. We combined both techniques to construct a novel method for computing quasi-periodic arcs in a two-parameter plane. It is an interesting and somewhat surprising fact that it actually enables the computation of quasi-periodic invariant tori with standard continuation software such as AUTO [16].

The computation of resonance surfaces presents a much harder problem and is the main topic of this paper. A preliminary version of our algorithm (11)–(18) for ODEs was published earlier in [35]. Since then we made many improvements, including the restriction to the fundamental domain, its extension to autonomous ODEs, a more general phase condition, adaptation and the new distance (10) that now takes the full orbit into account. These improvements resolved the computational problems observed in [35] for the 1/4 Arnol′d tongue.

The (α, s) parametrisation proposed in this paper extends the applicability of the previous methods from two-dimensional maps to general n-dimensional maps and ODEs. The (α, s) parametrisation is guaranteed to work for small coupling amplitude, but has the limitations discussed in Section 4.2, namely, that it cannot follow Arnol′d tongues that "bend back" in parameter space and that it generally does not provide a global parametrisation of 1/1, 1/2, 1/3, 2/3, 1/4 resonance surfaces, as was illustrated in Fig. 12. The first problem can often be solved by moving from the constant-α cross-section to a cross-section normal to a two-dimensional vector that reflects the average direction of the Arnol′d tongue in parameter space. This should work for high-period Arnol′d tongues, since their projection to the two-parameter plane often behaves like a "thick curve". Note that this modification seems straightforward but is not entirely trivial since the local parametrisation may become problematic if the centre of the circle of curvature of one of the boundary curves lies within

the tongue, which could happen at sharp turns. In that case, parts of the resonance surface may become covered multiple times and it is not clear how an arc-length continuation would behave.

A solution for the second problem was proposed in [32] by using a so-called $(\|f(x) - x\|, \phi)$ parametrisation ($\phi = \arg(f(x) - x)$) for planar maps. This approach successfully solves the global parametrisation problem for the caricature map, but this method no longer allows the straightforward computation of the boundaries of an Arnol'd tongue as the maximum and minimum of the parameter β with respect to arc-length. However, this idea can also be generalised from the (α, s) parametrisation of Eqs. (4)–(9) to a "$(\|f(x) - x\|, s)$ parametrisation", where α is now treated as a variable like β:

$$x_{1j}^q = f(x_{qj}^q, \alpha_j, \beta_j),$$
$$x_{2j}^q = f(x_{1j}^q, \alpha_j, \beta_j),$$
$$\vdots$$
$$x_{qj}^q = f(x_{q-1,j}^q, \alpha_j, \beta_j),$$
$$d(\xi_j, \xi_{j+1}) = h, \quad j = 1, \ldots, N-1,$$
$$d(\xi_N, \bar{\bar{\xi}}_1) = h,$$
$$\frac{1}{q} \sum_{i=1}^q \|f(x_{ij}^q, \alpha_j, \beta_j) - x_{ij}^q\|_2^2 = \gamma,$$
$$P(\xi) = 0.$$

This is a system of $nqN + N + N + 1$ equations for the $nqN + N + N + 2$ unknowns x_{ij}^q, α_j, β_j, h and γ, where d is a suitably defined distance. Note that the continuation parameter for computing the surface is γ. This $(\|f(x) - x\|, s)$ parametrisation may provide a valid global parametrisation in very general situations. In particular, it appears to be a good parametrisation, at least locally, for continuing from a p/q resonant Neimark–Sacker point by increasing γ from zero.

Despite the limitations outlined above, the algorithms and their possible generalisations presented in this paper are likely to work for many, if not most, practical applications. They are appealing because of their relative simplicity. All one needs is a one-parameter continuation software for two-point boundary value problems, for example AUTO [16].

Acknowledgements

References

[1] V.I. Arnol'd, Geometrical Methods in the Theory of Ordinary Differential EquationsGrundlehren der Mathematischen Wissenschaften [Fundamental Principles of Mathematical Science], vol. 250, Springer, New York, 1983, Translated from the Russian by Joseph Szücs, Translation edited by Mark Levi.
[2] D.G. Aronson, M.A. Chory, G.R. Hall, R.P. McGehee, Bifurcations from an invariant circle for two-parameter families of maps of the plane: a computer-assisted study, Commun. Math. Phys. 83 (3) (1982) 303–354.
[3] D.G. Aronson, M.A. Chory, G.R. Hall, R.P. McGehee, Resonance phenomena for two-parameter families of maps of the plane: uniqueness and nonuniqueness of rotation numbers, Nonlinear Dynamics and Turbulence, Interaction Mech. Math. Ser., Pitman, Boston, MA, 1983, pp. 35–47.
[4] P.L. Boyland, Bifurcations of circle maps: Arnol'd tongues, bistability and rotation intervals, Commun. Math. Phys. 106 (3) (1986) 53–381.
[5] H. Broer, C. Simó, J.C. Tatjer, Towards global models near homoclinic tangencies of dissipative diffeomorphisms, Nonlinearity 11 (3) (1998) 667–770.

[6] H.W. Broer, M. Golubitsky, G. Vegter, The geometry of resonance tongues: a singularity theory approach, Nonlinearity 16 (4) (2003) 1511–1538.

[7] H.W. Broer, G.B. Huitema, M.B. Sevryuk, Quasi-periodic motions in families of dynamical systems, Order amidst chaos Lecture Notes in Mathematics, vol. 1645, Springer, Berlin, 1996.

[8] H.W. Broer, G.B. Huitema, F. Takens, B.L.J. Braaksma, Unfoldings and bifurcations of quasi-periodic tori, Mem. Am. Math. Soc. 83 (421) (1990) viii+175.

[9] H.W. Broer, H.M. Osinga, G. Vegter, Algorithms for computing normally hyperbolic invariant manifolds, Z. Angew. Math. Phys. 48 (3) (1997) 480–524.

[10] E. Castellà, Á. Jorba, On the vertical families of two-dimensional tori near the triangular points of the bicircular problem, Celestial Mech. Dynam. Astronom. 76 (1) (2000) 35–54.

[11] T.N. Chan, Numerical bifurcation analysis of simple dynamical systems. Ph.D. Thesis, Department of Computer Science, Concordia University, Montreal, 1983.

[12] A. Chenciner, Bifurcations de points fixes elliptiques. II. Orbites periodiques et ensembles de Cantor invariants, Invent. Math. 80 (1) (1985) 81–106.

[13] H. Dankowicz, G. Thakur, A Newton method for locating invariant tori of maps, Int. J. Bifur. Chaos Appl. Sci. Eng. 16 (5) (2006) 1491–1503.

[14] W. de Melo, S. van Strien, One-dimensional Dynamics, Ergebnisse der Mathematik und ihrer Grenzgebiete (3) [Results in Mathematics and Related Areas (3)], vol. 25, Springer, Berlin, 1993.

[15] L. Dieci, J. Lorenz, Computation of invariant tori by the method of characteristics, SIAM J. Numer. Anal. 32 (5) (1995) 1436–1474.

[16] E. Doedel, A. Champneys, T. Fairgrieve, Y. Kuznetsov, B. Sandstede, X. Wang, Auto97: Continuation and bifurcation software for ordinary differential equations (with HomCont), Technical Report, Concordia University, 1997.

[17] J. Guckenheimer, P. Holmes, Nonlinear Oscillations, Dynamical Systems, and Bifurcations of Vector Fields, Applied Mathematical Sciences, vol. 42, Springer, New York, 1990 (revised and corrected reprint of the 1983 original).

[18] G.R. Hall, Resonance zones in two-parameter families of circle homeomorphisms, SIAM J. Math. Anal. 15 (6) (1984) 1075–1081.

[19] Á. Haro, R. de la Llave, A parameterization method for the computation of invariant tori and their whiskers in quasi periodic maps: numerical algorithms, Technical Report 04-350, Dynamical Systems Group, Barcelona UB-UPC, 2004.

[20] Á. Haro, R. de la Llave, A parameterization method for the computation of invariant tori and their whiskers in quasi periodic maps: rigorous results, Technical Report 04-348, Dynamical Systems Group, Barcelona UB-UPC, 2004.

[21] B. Hasselblatt, A. Katok, A First Course in Dynamics, Cambridge University Press, New York, 2003 (with a panorama of recent developments).

[22] Á. Jorba, Numerical computation of the normal behaviour of invariant curves of n-dimensional maps, Nonlinearity 14 (5) (2001) 943–976.

[23] C. Kaas-Petersen, Computation of quasiperiodic solutions of forced dissipative systems, J. Comput. Phys. 58 (3) (1985) 395–408.

[24] C. Kaas-Petersen, Computation of quasiperiodic solutions of forced dissipative systems, II, J. Comput. Phys. 64 (2) (1986) 433–442.

[25] I.G. Kevrekidis, R. Aris, L.D. Schmidt, S. Pelikan, Numerical computation of invariant circles of maps, Physica D 16 (2) (1985) 243–251.

[26] B. Krauskopf, Strong resonances and Takens's Utrecht preprint, in: H.W. Broer, B. Krauskopf, G. Vegter (Eds.), Global Analysis of Dynamical Systems, Inst. Phys., Bristol, 2001, pp. 89–111.

[27] R.P. McGehee, B.B. Peckham, Resonance surfaces for forced oscillators, Exp. Math. 3 (3) (1994) 221–244.

[28] R.P. McGehee, B.B. Peckham, Determining the global topology of resonance surfaces for periodically forced oscillator families, Normal Forms and Homoclinic Chaos (Waterloo, ON, 1992), Fields Inst. Commun., vol. 4, American Mathematical Society, Providence, RI, 1995, pp. 233–251.

[29] R.P. McGehee, B.B. Peckham, Arnold flames and resonance surface folds, Int. J. Bifur. Chaos Appl. Sci. Eng. 6 (2) (1996) 315–336.

[30] G. Moore, Geometric methods for computing invariant manifolds, Appl. Numer. Math. 17 (3) (1995) 319–331, Numerical methods for ordinary differential equations (Atlanta, GA, 1994).

[31] B.B. Peckham, The necessity of the Hopf bifurcation for periodically forced oscillators, Nonlinearity 3 (2) (1990) 261–280.

[32] B.B. Peckham, Global parametrization and computation of resonance surfaces for periodically forced oscillators, Numerical Methods for Bifurcation Problems and Large-scale Dynamical Systems (Minneapolis, MN, 1997), IMA Vol. Math. Appl., vol. 119, Springer, New York, 2000, pp. 385–405.

[33] B.B. Peckham, C.E. Frouzakis, I.G. Kevrekidis, Bananas and banana splits: A parametric degeneracy in the Hopf bifurcation for maps, SIAM J. Math. Anal. 26 (1) (1995) 190–217.

[34] R.H. Rand, P.J. Holmes, Bifurcation of periodic motions in two weakly coupled van der Pol oscillators, Int. J. Non-Linear Mech. 15 (4–5) (1980) 387–399.

[35] F. Schilder, Algorithms for Arnol′d tongues and quasi-periodic tori: A case study, Proceedings of the Fifth EUROMECH Nonlinear Dynamics Conference (ENOC-2005), 7–12 August 2005, Eindhofen, Eindhoven University of Technology, 2005.

[36] F. Schilder, H.M. Osinga, W. Vogt, Continuation of quasi-periodic invariant tori, SIAM J. Appl. Dyn. Syst. 4 (3) (2005) 459–488 (electronic).

[37] F. Takens, Forced oscillations and bifurcations, in: H.W. Broer, B. Krauskopf, G. Vegter (Eds.), Global Analysis of Dynamical Systems, Inst. Phys., Bristol, 2001, pp. 1–61.

[38] M. van Veldhuizen, A new algorithm for the numerical approximation of an invariant curve, SIAM J. Sci. Statist. Comput. 8 (6) (1987) 951–962.